Rate Constants for the Reactions of CH_3O with Cyclohexane, Cyclohexene, and 1,4-Cyclohexadiene: Variable Temperature Experiments and Theoretical Comparison of Addition and H-Abstraction Channels

Nathalie Gomez,*,†,‡ Eric Hénon,§ Frédéric Bohr,§ and Pascal Devolder†

Laboratoire de Physico-chimie des Processus de Combustion, UMR CNRS 8522, Centre d'Etudes et de Recherches Lasers et Applications, Université des Sciences et Technologies de Lille, 59655 Villeneuve d'Ascq Cedex, France, and Groupe de Spectroscopie Moléculaire et Atmosphérique, Laboratoire de Chimie-physique, UMR CNRS 6089, Faculté des Sciences, Université de Reims Champagne−Ardenne, Moulin de la Housse BP 1039, 51687 Reims Cedex 2, France

Received: January 18, 2001; In Final Form: July 18, 2001

First kinetic measurements for CH_3O reactions have been obtained for three cyclohydrocarbons using the discharge flow reactor combined with the laser induced fluorescence technique to detect CH_3O radicals over the pressure and temperature ranges 1−7 Torr of helium and 300−513 K. Measurements have been performed for the cyclohydrocarbons *c*-C_6H_{12} (k_1), *c*-C_6H_{10} (k_2), and 1,4-*c*-C_6H_8 (k_3). In addition to the experimental work, we have performed ab initio molecular orbital computations to get an insight into the mechanism of the three reactions, using PMP2, HF-DFT (B3LYP), and CASPT2 methods. The rate constant k_1 has been calculated using the Transition State Theory. Measured rate constants are pressure independent in our experimental range. Arrhenius expressions are (k_i in cm^3 s^{-1}) $k_1 = 8.8\binom{+11.0}{-5.0} \times 10^{-12}$ exp[−(24.5 ± 3.0) kJ mol^{-1}/*RT*] (403−513 K), $k_2 = (3.1 \pm 0.8) \times 10^{-12}$ exp[−(15.3 ± 0.8) kJ mol^{-1}/*RT*] (300−503 K), and $k_3 = 1.9\binom{+1.6}{-0.9} \times 10^{-12}$ exp[−(7.6 ± 1.9) kJ mol^{-1}/*RT*] (300−513 K). A good agreement between the experimental and theoretical rate constants k_1 has been found. The comparison between the computed and the experimentally determined barrier heights serves as an endorsement of the increasing reactivity in the series from cyclohexane system to the 1,4-cyclohexadiene system.

1. Introduction

The alkoxyl radicals are important intermediate species during oxidation of VOC (Volatile Organic Compounds) in atmospheric chemistry.[1] In the atmosphere, they may exhibit three reaction channels: reaction with O_2 (giving a carbonyl and HO_2 radical), decomposition (giving a carbonyl and an alkyl radical), or isomerization into an hydroxy-alkyl radical:

$$RO + O_2 \rightarrow R'CHO + HO_2$$

$$RO \rightarrow R'CHO + R''$$

$$RO \rightarrow R'OH$$

The first channel (oxidation by atmospheric oxygen) is the dominant one for small alkoxyl radicals (number of carbon atoms C < 4). The isomerization of alkoxyl radicals through intramolecular H atom transfer plays an important role in the degradation of higher alkoxyl radicals (number of carbon atoms C ≥ 4). Direct experimental measurements of the latter rate constants are difficult.[2,3]

Baldwin et al.[4] suggested that the barrier to isomerization could be thought as the sum of two contributions: (i) the ring strain energy and (ii) the barrier energy of a corresponding bimolecular abstraction reaction in which a H atom is transferred from a carbon atom to an oxygen atom. According to that idea, Atkinson[1] has estimated the isomerization barriers in alkoxyl radicals by analogy with OH bimolecular abstraction barriers. More recently, quantum chemistry calculations by Viskolcz et al.[5] and Lendvay and Viskolcz[6] have shown on a more quantitative basis that these qualitative rules for H atom transfer reactions were well observed for isomerization of a few alkyl radicals and of the 1-butoxyl radical. Because the ring strain energy mainly depends on the size of the ring and not on its nature, it is easy to estimate this energy. Only the measurement of abstraction parameters is required to be able to estimate the isomerization parameters.

In line with the estimation of the isomerization rate parameters for large alkoxyl radicals, the aim of this study is the derivation of accurate values for activation energies of a few characteristic abstraction reactions of alkoxyl radicals. At room temperature, however we were unable to obtain sizable data for the reactions of CH_3O with two linear alkanes as reactants: ethane (H bonded to a primary C) and octane (H bonded to a primary or a secondary C); the former reaction rate was too slow even at 500 K. In parallel, at room temperature, Biggs et al.[7] estimated a small upper limit of rate constants for similar reactions. Because these reactions have proved to be slow at room temperature, experiments at higher temperatures had to be performed. These conditions restricted the measurements to methoxyl radical (CH_3O) because larger alkoxyl radicals (ethoxyl and propoxyl) already exhibit a significant unimolecular decomposition at moderate temperatures.[8,9]

* To whom correspondence should be addressed. E-mail: nathalie.gomez@univ-reims.fr. E-mail: pascal.devolder@univ-lille1.fr. Fax: (33) (0)3 20 43 69 77. E-mail: eric.henon@univ-reims.fr. E-mail: frederic.bohr@univ-reims.fr Fax: (33) (0)3 26 91 33 33.

† Université des Sciences et Technologies de Lille.

‡ Present address: G.S.M.A., Laboratoire de Chimie-physique, UMR CNRS 6089, Faculté des Sciences, Université de Reims Champagne−Ardenne, Moulin de la Housse BP 1039, 51687 Reims Cedex 2, France.

§ Université de Reims Champagne−Ardenne.

10.1021/jp010204h CCC: $20.00
Published on Web 11/27/2001

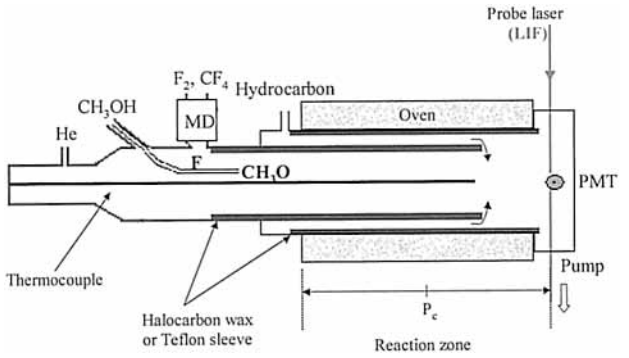

Figure 1. Schematic diagram of the discharge flow apparatus (MD, microwave discharge; PMT, photomultiplier).

Therefore, the title six-membered ring reactants have been selected for the following reasons: (i) like for OH abstraction reactions, the large number of abstractable H atoms in cyclohexane leads to a measurable rate constant corresponding to a H atom transfer where the H atom is bonded to a secondary C and (ii) cyclohexene and 1,4-cyclohexadiene were selected because the presence of allylic hydrogen atoms should enhance the rate constants for abstraction. So we have examined the case of these three cyclohydrocarbons, i.e., the following reactions:

$$CH_3O + c\text{-}C_6H_{12} \rightarrow \text{products 1} \quad (1)$$

$$CH_3O + c\text{-}C_6H_{10} \rightarrow \text{products 2} \quad (2)$$

$$CH_3O + 1,4\text{-}c\text{-}C_6H_8 \rightarrow \text{products 3} \quad (3)$$

Concerning the reaction mechanisms, only the abstraction of an hydrogen atom occurs for c-C_6H_{12}, whereas for c-C_6H_{10} and 1,4-c-C_6H_8, addition on the double bond may play a role. In parallel with variable pressure measurements (to check for falloff behavior), high level quantum calculations have been performed with two objectives: (i) to elucidate the mechanism and (ii) to compare with experimental results on a quantitative basis.

Section 2 gives a description of the experimental features and results: apparatus, rate constant treatment, and experimental conditions. Section 3 of this paper gives the ab initio details as well as results for the location and the characterization of the relevant stationary points on the potential energy surface. Results of these calculations provide the starting point for computational methods of the reaction rate using energy differences at a higher level of theory. The corresponding computational details are provided in section 4, together with those for Transition State Theory (TST)[10] rate constant calculations. The experimental and the theoretical results are compared and discussed in section 5, whereas section 6 summarizes the results and the concluding remarks.

2. Experimental Study

2.1. Apparatus and Chemicals. The reactor, made of Pyrex, had an internal diameter of about 2 cm and was 70 cm long. It can be electrically heated by an oven, and gases temperature has been monitored by a thermocouple located directly in the reaction zone inside the injector. Several configurations of the setup could be used (fixed or movable discharge). The movable discharge configuration (Figure 1) was chosen to perform most experiments. In this technique, the microwave discharge was switched on in a sidearm connected to the movable injector providing a constant methoxyl radical concentration [CH_3O] at the exit of the injector. To avoid excessive loss of the CH_3O radicals on walls, the injector and the reactor were either internally coated with halocarbon wax ($T < 393$ K) or covered by a thin Teflon sleeve ($T < 523$ K). Every gas flow was regulated by a calibrated mass flow meter (Tylan FC-260), but the reactant/He flow rate was also deduced from the measurement of the rate of pressure increase in a calibrated (closed) volume.

The CH_3O radical concentration was measured by LIF technique using a tunable dye laser 50 pumped by a frequency doubled YAG 781-C, both Quantel laser. The fluorescence-excitation spectrum recorded in the 287−300 nm range for the methoxyl radical was identical to the previous reported by Inoue et al.[11] In our experiments, we monitored CH_3O radicals by the excitation of the (A^2A_1, $v' = 4 \leftarrow X^2E$, $v'' = 0$) transition corresponding to an excitation wavelength around 293 nm. We assumed that the integrated LIF signal was linearly dependent on the CH_3O radical concentration for unsaturated transition (this was checked before). A spherical excitation beam was obtained with collimators which also decreased interference light due to the probe beam and reduced light scattered by windows.[12,13] The fluorescence was collected perpendicularly to the excitation laser beam using a Hamamatsu R212UH photomultiplier: for this, focalization lenses and an Oriel cutoff filter at $\lambda > 305$ nm were used. The signal of CH_3O was displayed on a fast scope and integrated by a EG&G PAR 162/165 boxcar averager connected to a computer for the acquisition data and kinetic analysis. In general, the delay between the laser pulse and the opening of the boxcar gate was 200 ns, and the gate width was 50 ns.

The carrier gas helium (99.995%, Air Liquide) flowed through a molecular sieve held at 77 K to remove water and through a liquid nitrogen trap. F_2 (5% in helium, Air Liquide) and CF_4 (99.995%, Alphagaz) flowed through a 77 K trap before being stored (highly diluted in helium, ca. 0.05 to 2%) in Pyrex balloons. Methanol/He mixtures were generated by saturation of a helium flow with methanol, whereas the three reactant flow rates were regulated by needle valves and directly pomped from the liquid thermostated at 303 K. Methanol (> 99.8%, SDS), cyclohexane (≥ 99.5%, Fluka), cyclohexene (≥ 99%, Fluka), and 1,4-cyclohexadiene (97%, Aldrich) were carefully degassed before use.

2.2. Radical Generation. Methoxyl radicals are usually generated in the movable injector by the fast $CH_3OH + F$ reaction. Fluorine atoms are prepared by a microwave discharge in F_2/He or CF_4/He mixtures flowing through Al_2O_3 ceramic to reduce F atoms reactions at the surface. This reaction leads to two radicals (CH_3O and CH_2OH) in roughly equivalent yields (ca. 0.5 ± 0.1) over a large range of temperatures.[14,15] Typical concentrations for CF_4 (or F_2) and CH_3OH were about $(1-10) \times 10^{12}$ cm^{-3} and 10^{14} cm^{-3}, respectively, leading to about 5×10^{11} cm^{-3} CH_3O radicals; a large excess of methanol was used to avoid the fast $CH_3O + F$ reaction. A clean source of CH_3O radicals[16] was used in a few experiments to control the role of hydroxymethyl radicals in the kinetics:

$$F + CH_4 \rightarrow CH_3 + HF$$

$$CH_3 + NO_2 \rightarrow CH_3O + NO$$

In varying the NO_2 flow rate (CH_3 radicals in excess), this sequence also allowed us to estimate the CH_3O concentration in the reactor.[17] The detection limit was estimated to be [CH_3O] $= 10^{10}$ cm^{-3} for a signal-to-noise ratio of unity.

2.3. Determination of Rate Constants. Experimental studies of reactions 1−3 have been performed in the pseudo-first-order approximation with a large excess of reactant; total pressure

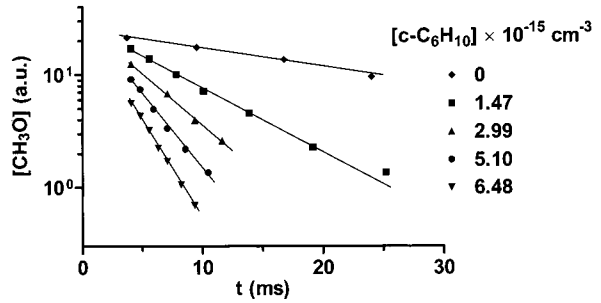

Figure 2. Semilogarithmic plots of the CH_3O LIF signal versus reaction time for reaction 2 at 483 K and 4.03 Torr for different *c*-C_6H_{10} concentrations (in 10^{15} cm^{-3}; solid lines, linear least squares).

TABLE 1: Experimental Conditions (Concentrations in cm^{-3})

	c-C_6H_{12} (1)	*c*-C_6H_{10} (2)	1,4-*c*-C_6H_8 (3)
T (K)	403−513	300−503	300−513
P_c (Torr)	≈4	1−7	1−3
v (cm s^{-1})	≈1300	1000−6700	2500−3000
[reactant] × 10^{-15}	< 15	< 14	< 2.5

was within the 1−7 Torr of helium range, and the temperature within the 300−513 K range; the gas flow velocity varied between 1000 and 6700 cm s^{-1}. The range of experimental parameters are presented in Table 1 for reactions 1−3.

To obtain the true first-order rate constant $k^{(1)}$, two corrections have been applied to the observed decay rate k_{obs}: (i) Poiseuille law inducing a pressure gradient (directly measured) along the reactor has been taken into account by adopting as "corrected" pressure (P_c) the pressure in the middle of the reaction zone (see Figure 1) and (ii) axial and radial diffusions of the CH_3O radicals in helium have been calculated according to eqs I and II[18]:

$$D_{Pc,T} = 457\left(\frac{1}{P_c(\text{Torr})}\right)\left(\frac{T(\text{K})}{298}\right)^{3/2} \quad \text{(I)}$$

$$k^{(1)} = k_{obs}\left(1 + \frac{k_{obs}D_{Pc,T}}{v^2} + \frac{k_{obs}R^2}{48D_{Pc,T}}\right) \quad \text{(II)}$$

with v (cm s^{-1}), R (cm), and $D_{Pc,T}$ (cm^2 s^{-1}) being the mean flow velocity, the reactor radius, and the diffusion coefficient, respectively. To calculate $D_{Pc,T}$ (eq I), we adopted the value of 457 cm^2 s^{-1} at 298 K and 1 Torr.[19] We measured k_{obs} for 6−10 reactant concentrations (including zero), and the corresponding $k^{(1)}$ values were derived in applying of the corrections discussed above (eqs I and II). A plot of $k^{(1)}$ versus the reactant concentrations provides (i) the bimolecular rate constant k as the slope and (ii) the wall decay rate constant k_w as the intercept. All uncertainties in the rate constants reported in this paper are statistical (two standard deviations).

Typical records of decay curves (log[CH_3O] versus reaction time) for different *c*-C_6H_{10} concentrations as well as first-order rate constant $k_2^{(1)}$ against [*c*-C_6H_{10}] at different temperatures are displayed in Figure 2 and 3, respectively.

All decay plots such as in Figure 2 (i.e., log [CH_3O] versus reaction time) showed exponential decays. Well behaved kinetics have also been observed with the two other reactants. Furthermore, wall decay rate constants obtained from intercept in pseudo-first-order plots (Figure 3) are close to the measured values at zero reactant concentration (k^0_w). This comparison provides a good test for the self-consistency of the experimental data. The wall decay rate constant included both the loss of

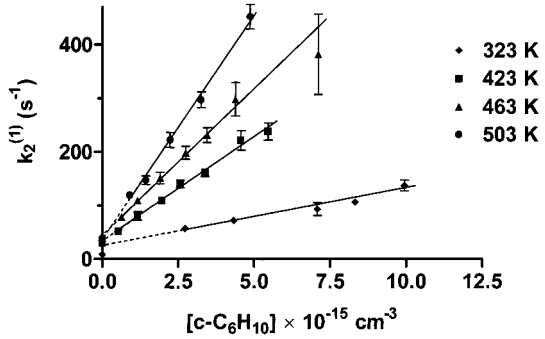

Figure 3. Pseudo-first-order rate constants for reaction 2 plotted as a function of [*c*-C_6H_{10}] for different temperatures.

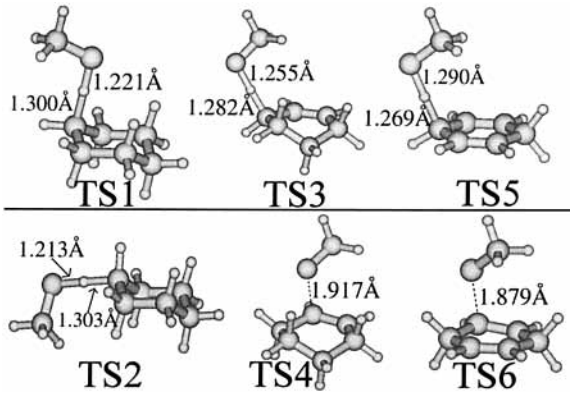

Figure 4. UHF/cc-pVDZ optimized geometries of transition states for reactions 1 (abstraction, TS1 for axial hydrogen atom and TS2 for equatorial hydrogen atom), for reaction 2 (abstraction, TS3; addition, TS4), for reaction 3 (abstraction, TS5; addition, TS6). The distances are in angstroms.

CH_3O radicals on the wall and undesirable secondary reactions. The typical values for k^0_w are in the range of 30−40 s^{-1}, independent of temperature. It is interesting to note that *c*-C_6H_{10} and 1,4-*c*-C_6H_8 can polymerize or isomerize in liquid phase. To avoid this, a stabilizing agent (2,6-diterbutyl-*p*-cresol = ionol) is added by the supplier. However, we can compare the vapor pressure at 303 K (reactant ≈ 100 Torr, ionol ≈ 0.03 Torr) and conclude that the molar fraction of ionol is negligible in the gas phase. To make sure that this agent does not disturb our kinetic investigations, a few experiments have been conducted with distilled reactants; no change was observed for rate constants.

3. Molecular Structure Calculations

3.1. Computational Details. Ab initio and HF-DFT calculations were performed using the Gaussian 94 package.[20] The structures of reactants and transition state were fully optimized using the analytical gradients at two levels of theory: UHF and HF-DFT (B3LYP[21−23]), using the cc-pVDZ basis set.[24−26] The calculations for the reactants were done as those for supermolecules with the molecular fragments placed 100 Å apart. The minimum energy path (MEP) was determined by the IRC technique to check whether the transition state links the proper reactants and products. Vibrational frequencies were determined within the harmonic approximation at two levels of theory, namely, UHF and HF-DFT (B3LYP) levels, using the corresponding geometries. Figure 4, showing the transition state (TS) structures, has been obtained using the Molden package.[27] Transition state species notation appears in this figure.

3.2. Geometrical Features. All of the transition states found are shown in Figure 4. Concerning the H atom abstraction from

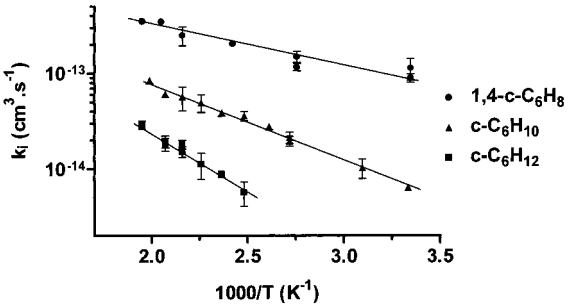

Figure 5. Arrhenius plots for CH_3O + *c*-C_6H_{12}, CH_3O + *c*-C_6H_{10}, and CH_3O + 1,4-*c*-C_6H_8 reactions.

TABLE 2: Optimized Geometrical Parameters of the Reactants (Distances in Angstrom, Angles in Degree)

parameter	UHF	HF-DFT(B3LYP)
	CH_3O	
C−O	1.378	1.364
	Cyclohexane	
C−H	1.097	1.107
C−C	1.531	1.536
	Cyclohexene	
C═C	1.325	1.340
(C═)C−H	1.085	1.096
C−H (α)	1.094	1.108
∠C−C═C	123.6	123.4
∠H−C═C	119.3	119.4
∠H−C═C−C	-179.9	179.9
	1,4-Cyclohexadiene	
C═C	1.323	1.338
(C═)C−H	1.085	1.095
C−*H* (α)	1.096	1.109
∠C−C═C	123.7	123.5
∠H−C═C	119.5	119.6
∠H−C═C−C	180.0	180.0

cyclohexane (the only possible channel for reaction 1), two transition state structures, namely TS1 and TS2, have been found involving either the axial or equatorial hydrogen atom, respectively. For reaction 2 involving cyclohexene, the TS3 and TS4 transition states correspond to the abstraction and addition channels, respectively. For reaction 3, the TS5 and TS6 transition states represent the abstraction and addition channels, respectively. In Tables 2 (reactants), 3 (TS1, TS2, TS3, TS5), and 4 (TS4, TS6), we give the geometrical parameters for the reactants, the abstraction, and the addition transition states involved in the aforementioned reactions, respectively.

The two corresponding TS1 and TS2 energies are very close (the energy difference being about 4 kJ mol^{-1} at the HF-DFT (B3LYP) level of theory, which is an usual uncertainty for computed activation energies). Only the axial results (the lower energy) will be used subsequently. For each channel (addition or abstraction) of reactions 2 and 3, it is interesting to note that only one relative approach of CH_3O is obtained. The addition channels (TS4 and TS6) show a rather low imaginary vibrational frequency compared to the abstraction channel (TS3 and TS5) and due to the long distance O···C (about 2.0 Å) in the addition transition state structures.

Our theoretical investigations have revealed the active role played by the π electrons in the reaction mechanism. Inspection of the transition state structures for abstraction (TS1, TS2, and TS3) displayed in Figure 4 shows that the CH_3 fragment of CH_3O takes place above the cyclic hydrocarbon only for cyclohexene and 1,4-cyclohexadiene (what we call the "scorpion" effect). On the contrary, the CH_3 fragment is always located outside of the ring structure for the reaction involving

TABLE 3: Optimized Geometrical Parameters of Transition States (TS1, TS2, TS3, and TS5) for H-Abstraction Pathways (Distances in Angstrom, Angles in Degree, and Imaginary Frequencies in cm^{-1})

parameter	UHF	HF-DFT (B3LYP)
	CH_3O + Cyclohexane	
	axial (equatorial)	
	TS1 (TS2)	
O···H	1.221 (1.213)	1.280 (1.262)
H···C	1.300 (1.303)	1.261 (1.268)
C−O	1.393 (1.392)	1.398 (1.396)
∠O···H···C	178.5 (177.6)	174.6 (176.8)
∠H···C−C	105.2 (107.8)	104.6 (108.6)
∠C−O···H	106.5 (107.4)	107.7 (108.4)
∠C−O···H···C	−62.4 (77.4)	−81.7 (−0.5)
∠O···H···C−C	−156.8 (3.7)	−110.4 (62.5)
im. freq.	2851i (2894i)[a]	1276i (1349i)
	CH_3O + Cyclohexene	
	TS3	
O···H	1.255	1.367
H···C	1.282	1.218
C−O	1.391	1.388
∠O···H···C	174.2	171.2
∠H···C−C	108.0	107.9
∠C−O···H	106.1	107.4
∠C−O···H···C	80.1	55.6
∠O···H···C−C	−92.3	−84.2
im. freq.	2885i[a]	874i
	CH_3O + 1,4-Cyclohexadiene	
	TS5	
O···H	1.290	1.499
H···C	1.269	1.176
C−O	1.391	1.381
∠O···H···C	178.1	171.9
∠H···C−C	107.2	108.1
∠C−O···H	105.4	106.7
∠C−O···H···C	0.0	−0.1
∠O···H···C−C	−62.0	−62.0
im. freq.	2820i[a]	356i

[a] Scaled by 0.89.

cyclohexane (TS1). The same effect is observed for the addition channel: the 1,4-cyclohexadiene transition state structure (TS6) shows a CH_3 fragment of CH_3O above the ring and between the two π bonds, whereas for the cyclohexene system (TS4), the CH_3 fragment lies slightly outside the ring but remains close to the π bond.

4. Electronic Energy and TST Rate Constants: Computational Details

In many cases, it is desirable to obtain energy differences at a high level of theory such as MP4 or CASPT2 for example, particularly to carry out rate constant calculations through TST at a later stage. The cost of optimizing geometries at these levels can be prohibitive. In these conditions, it is helpful to do calculations at a higher level of theory using the geometries optimized at a lower level. Ab initio calculations were performed using the Gaussian 94[20] and MOLCAS4[28] packages.

At first, MP2 and MP4(SDQ) calculations were carried out using the cc-pVDZ basis set, i.e., Möller−Plesset perturbation theory at the second order and at the fourth order, respectively, including the effects of all single, double, and quadruple excitations and using the previously described UHF geometries. For open shell structures, the spin contamination[29] has been taken into account in the MP2 calculation of the energies using a projection method included in the Gaussian program; the corresponding results will be noted PMP2.

TABLE 4: Optimized Geometrical Parameters of Transition States (TS4 and TS6) for Addition Pathways (Distances in Angstrom, Angles in Degree, and Imaginary Frequencies in cm^{-1})

parameter	UHF	HF-DFT (B3LYP)
CH_3O + Cyclohexene		
TS4		
O···C	1.917	2.082
C−O	1.388	1.386
C = C	1.403	1.372
∠O···C=C	105.0	98.6
∠C−O···C	113.0	114.5
∠H−C=C	117.0	118.7
∠O···C=C−C	83.9	88.2
∠C−O···C=C	57.8	68.5
∠H−C=C−C	−171.6	−174.4
im. freq.	591i[a]	306i
CH_3O + 1,4-Cyclohexadiene		
TS6		
O···C	1.8790	2.0239
C−O	1.3903	1.3894
C=C	1.4059	1.3759
∠O···C=C	107.4	100.4
∠C−O···C	116.1	115.7
∠H−C=C	116.3	118.3
∠O···C=C−C	94.6	98.5
∠C−O···C=C	−35.1	−62.4
∠H−C=C−C	−166.8	−171.7
im. freq.	645i[a]	375i

[a] Scaled by 0.89.

The HF-DFT method has also been employed with the B3LYP exchange-correlation functional[21−23] and with the cc-pVDZ basis set, using the previously described HF-DFT geometries.

At last, the CASPT2 method was carried out to incorporate both dynamic and non dynamic correlation effects on the relative energy ordering of the calculated stationary points. The CASPT2 approach[30−33] is based on a second-order perturbation treatment where the CASSCF wave function is taken as the reference function. Thus, the parameters of the CASPT2/CASSCF calculations are those of the CASSCF step. In this study, single-point CASPT2/CAS(3,3) were obtained using again cc-pVDZ basis set on the UHF/cc-pVDZ optimized geometries and excluding innershells and corresponding virtual counterpart from the perturbation calculation.

For the abstraction mechanism, the active space (3,3) that best describes the C−H bond breaking and O−H bond forming includes the σ_{C-H} bonding molecular orbital (MO) with the associated σ^*_{C-H} antibonding MO and the single electron MO. As for the addition mechanism, the active space (3,3) that best describes the π bond breaking and C−O bond forming consists of the bonding $\pi_{C=C}$ and antibonding $\pi^*_{C=C}$ MOs and the single electron MO.

Rate constant calculations were done by carrying out the TST[10] by using the KISTHEP[34] and POLYRATE[35] packages. In TST, the transition state is assumed to be at the saddle point on the reaction path, and the rate constant for a bimolecular gas-phase reaction is calculated by eq III:

$$k^{TST}(T) = \frac{k_b T}{h}\left(\frac{RT}{P_0}\right)\exp[-\Delta G^{0\ddagger}(T)/RT] \qquad \text{(III)}$$

In this equation, k_b is the Boltzmann constant, T is the temperature, h is the Planck's constant, $\Delta G^{0\ddagger}$ is the Gibbs free-energy of activation, R is the ideal gas constant, and P_0 is the one bar standard state pressure. The simple Wigner formula for the tunneling correction[36] in conventional TST, though approximate, has been applied. The corresponding rate constant is denoted TST/W in this paper. Semiclassical transmission coefficients within the zero curvature approximation[37−40] were calculated using the POLYRATE program[35] with the vibrationally adiabatic ground-state potential: $V^G_a(s) = V_{MEP}(s) + ZPE(s)$ where the classical potential energy $V_{MEP}(s)$ at s (the reaction coordinate) is represented by an Eckart function and $ZPE(s)$ denotes the zero-point energy in vibrational modes that are transverse to the MEP. The corresponding rate constant is denoted TST/MEPSAG in this paper. Our rate constant calculations are based on higher-level single-point CASPT2/cc-pVDZ energies using the lower-level UHF/cc-pVDZ geometries with UHF/cc-pVDZ frequencies.

TABLE 5: Experimental Data at Different Temperatures (k_i in 10^{-14} cm^3 s^{-1})

T (K)	k_1	k_2	k_3
299			10.10 ± 2.90
300		0.64 ± 0.02	
323		1.03 ± 0.24	
363			13.25 ± 2.00
368		2.04 ± 0.29	
383		2.79 ± 0.22	
403	0.57 ± 0.16	3.59 ± 0.40	
413			20.30 ± 0.90
423	0.88 ± 0.07	3.86 ± 0.30	
443	1.12 ± 0.34	4.92 ± 1.02	
463	1.65 ± 0.19	5.67 ± 1.58	25.00 ± 5.60
483	1.87 ± 0.28	6.09 ± 0.49	
488			34.50 ± 2.00
503		8.47 ± 0.68	
513	2.89 ± 0.29		35.10 ± 1.00

5. Discussion

The measured rate constants for reactions 1−3 are gathered in Table 5: all reported data have been obtained with the F + CH_3OH source. In this table, we do not distinguish rate constants at different pressure because of their similar values and the small pressure range. Their temperature dependence obeys simple Arrhenius equations obtained by linear least-squares analysis (k_i in cm^3 s^{-1}):

$$k_1 = 8.8\left(^{+11.0}_{-5.0}\right) \times 10^{-12}\exp[-(24.5 \pm 3.0)\ \text{kJ mol}^{-1}/RT] \qquad 403 < T\,(\text{K}) < 513$$

$$k_2 = (3.1 \pm 0.8) \times 10^{-12}\exp[-(15.3 \pm 0.8)\ \text{kJ mol}^{-1}/RT] \qquad 300 < T\,(\text{K}) < 503$$

$$k_3 = 1.9\left(^{+1.6}_{-0.9}\right) \times 10^{-12}\exp[-(7.6 \pm 1.9)\ \text{kJ mol}^{-1}/RT] \qquad 300 < T\,(\text{K}) < 513$$

The corresponding Arrhenius plots are presented in Figure 5.

No direct comparison with litterature data could be made because of a lack of published data concerning the reactions of the CH_3O radical with cyclohydrocarbons. Consequently, our results are discussed on the basis of data concerned with similar reactions involving either the CH_3O radical or the cyclohydrocarbons. Next, theoretical results are presented for comparison with experimental ones.

The only available data concerning H atom transfer reactions of CH_3O radical with a few VOC have been reviewed a few years ago by Heicklen;[3] they were based either on indirect measurements (for example from reverse reaction rate constants) or on relative ones (with estimation of competing radical + radical reactions such as $CH_3O + CH_3 \rightarrow CH_3OCH_3$). Concern-

TABLE 6: Computed Barrier Heights in kJ mol^{-1} Using cc-pVDZ Basis Set (Without Zero-Point Energy Corrections in Brackets)

	cyclohexane	cyclohexene		1,4-cyclohexadiene	
method		abstraction	addition	abstraction	addition
UMP2	18.4 (25.9)	30.9 (40.5)	27.6 (23.0)	32.6 (43.9)	32.6 (27.6)
UMP4(SDQ)	35.5 (43.0)	39.7 (49.3)	27.6 (23.0)	34.3 (45.6)	34.7 (29.7)
PMP2	5.8 (13.4)	−5.8 (3.8)	−14.2 (−18.8)	−24.2 (−12.9)	−8.8 (−13.8)
HF-DFT (B3LYP)	10.4 (17.1)	3.8 (8.8)	2.1 (−2.9)	−7.1 (−5.4)	13.4 (5.0)
CASPT2	18.4 (25.9)	−7.9 (1.7)	−14.6 (−19.2)	−26.3 (−15.0)	−7.5 (−12.5)
exp. (E_a)	24.5 (403−513 K)	15.3 (300−503 K)		7.6 (300−513 K)	

TABLE 7: Computed Transition-State Rate Constants (cm^3 s^{-1}) for Reaction 1 Using MP4, HF-DFT(B3LYP) and CASPT2 Potential Informations[a]

	MP4	HF-DFT(B3LYP)	CASPT2			exp.
T (K)	TST	TST	TST	TST/W	TST/MEPSAG	
400	2.310×10^{-17}	1.611×10^{-14}	4.042×10^{-15}	2.175×10^{-14}	2.778×10^{-14}	5.539×10^{-15}
420	4.307×10^{-17}	2.091×10^{-14}	5.893×10^{-15}	2.931×10^{-14}	3.438×10^{-14}	7.868×10^{-15}
440	7.644×10^{-17}	2.667×10^{-14}	8.363×10^{-15}	3.865×10^{-14}	4.223×10^{-14}	1.083×10^{-14}
460	1.299×10^{-17}	3.353×10^{-14}	1.159×10^{-14}	4.999×10^{-14}	5.150×10^{-14}	1.449×10^{-14}
480	2.126×10^{-16}	4.160×10^{-14}	1.573×10^{-14}	6.358×10^{-14}	6.238×10^{-14}	1.892×10^{-14}
500	3.363×10^{-16}	5.101×10^{-14}	2.095×10^{-14}	7.969×10^{-14}	7.508×10^{-14}	2.419×10^{-14}
520	5.163×10^{-16}	6.189×10^{-14}	2.743×10^{-14}	9.856×10^{-14}	8.981×10^{-14}	3.035×10^{-14}

[a] The experimental values are given for comparison.

ing the barriers, the recommended values range from 12 kJ mol^{-1} ($CH_3O + n$-C_4H_{10}) to 30 kJ mol^{-1} ($CH_3O + C_2H_6$). The values determined in this work are in the same range. An upper limit of the rate constant for the reaction $CH_3O + c$-$C_6H_{12} \rightarrow$ products 1 has been estimated in a previous study using the laser photolysis/LIF technique:[2] k_1 (356 K) $< 2.5 \times 10^{-15}$ cm^3 s^{-1}. This upper limit is in agreement with the value deduced from our Arrhenius expression (k_1 (356 K) $= 2.2 \times 10^{-15}$ cm^3 s^{-1}). Furthermore these two results were determined using two different direct experimental techniques and two different sources for the CH_3O radicals.

It is interesting to compare the reactivity of the CH_3O radical with that of the OH radical, for which there is a wealth of data. With the alkenes, the reactions of OH at room temperature are considered to be mainly addition ones, with a possible small contribution of the abstraction channel. The recommended values with the same reactants[41] at 760 Torr and 298 K are (in cm^3 s^{-1}): 7.2×10^{-12} (OH + c-C_6H_{12}), 6.8×10^{-11} (OH + c-C_6H_{10}), and 9.9×10^{-11} (OH + 1,4-c-C_6H_8). It is not clear however whether the presence of very labile allylic H atoms in the two alkenes could strongly enhance the abstraction pathway. From a smog chamber study of the products of the reaction OH + 1,4-c-$C_6H_8 \rightarrow$ products, Ohta[42] concluded that the abstraction channel amounts to 15% of the total reaction rate. Furthermore, many rate constants for the reaction of the OH radical with alkenes exhibit a weak or a negative temperature coefficient, in contrast with the temperature coefficients observed for reactions 1−3 in the present work. Finally, in the same study, Ohta[42] detected the presence of an abstraction product (CH_3OH) assigned to the channel (CH_3O + 1,4-c-$C_6H_8 \rightarrow CH_3OH$ + products) and suggested that "CH_3O abstracts hydrogen from 1,4-c-C_6H_8 more preferably than OH".

From this discussion, together with the lack of pressure dependence in our small pressure range and the observation of a clear positive temperature coefficient in our experiments, we would favor the abstraction channel as the major reaction pathway in the reactions of CH_3O with the two alkenes as well.

To provide further insight into the mechanism, quantum chemistry calculations have been performed in connection with our previous investigation of the reaction $CH_3O + HCH(O) \rightarrow CH_3OH + HCO$.[2,43,44]

The electronic barrier heights (in kJ mol^{-1}) obtained at different levels of theory are listed in Table 6 and compared with our experimental activation energies. UMP2 and UMP4 electronic activation energies are similar except for the cyclohexane system. We observe a large spin contamination at the UMP2 level of theory, the effect of which leads to negative energy barriers for unsaturated systems at the corrected PMP2 level of theory. Negative barrier heights are observed also with the CASPT2 and HF-DFT methods (the effect is less important with this latter method), mainly for the 1,4-cyclohexadiene system. One reason could be the probable existence of a long distance complex (not found at the UHF level in this work) that should be examined at a higher level of theory (MP2 optimization for example). However, this requires a large demanding computation time for these large systems.

According to the two last methods (PMP2 and CASPT2), the H-abstraction pathway on cyclohexane appears to have the largest electronic activation energy, this corroborates our experimental results. With cyclohexene, it is apparent that the abstraction and the addition pathways have relatively close electronic activation energies. With 1,4-cyclohexadiene, the ZPE correction emphazises the initially dominant channel: the abstraction channel is the more favorable one. One reason could be the loss of the planar structure and part of the π system in the case of the addition process.

TST rate constants are reported in Table 7 for reaction 1, the only one for which positive activation energies have been found (see Table 6). The direct comparison with experiment is possible in this case because only the H-abstraction process occurs. Inspection of Table 7 and Arrhenius plot (Figure 6) show that, while the HF-DFT and MP4 methods overestimates and underestimates the rate constant, respectively, the CASPT2 method compares well with the experimental data; for example, at 450 K, $k^{TST} = 0.99 \times 10^{-14}$ cm^3 s^{-1} and $k^{exp} = 1.27 \times 10^{-14}$ cm^3 s^{-1}. The Arrhenius activation energy obtained from TST rate constants using CASPT2 (27.6 kJ mol^{-1}) in the experimental temperature range is very close to the experimental one (24.5 kJ mol^{-1}). Moreover, the theoretical and experimental frequency factors are of the same order of magnitude: 1.6×10^{-11} cm^3 s^{-1} and 8.8×10^{-12} cm^3 s^{-1}, respectively. The ZCT/SAG (zero curvature tunneling) correction computed by using

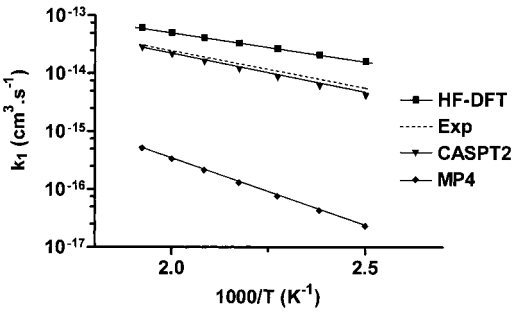

Figure 6. Comparison of the computed rate constants for reaction 1 by the TST formalism.

the POLYRATE program, κ (400 K) = 6.3 and κ (500 K) = 3.3, tends to shift the theoretical value from that onserved experimentally. Variational effect still needs to be estimated before to discuss about the CASPT2 values.

To conclude, CASPT2 calculations provide a good agreement with experiments for reaction 1. There is no dominant channel for reaction 2, whereas for reaction 3, the abstraction channel seems to be more favored than the addition one. Further calculations need to be done to evaluate the influence of the correlation effect at the geometry optimization step and next at the energy determination. It would be also useful to check for the possible existence of long distance intermediate complexes which could explain some theoretical negative barrier heights derived from a few methods for unsaturated compounds.

6. Conclusion

We have performed the first extented measurements of the rate constants for the reactions of CH_3O with the three cyclohydrocarbons: *c*-C_6H_{12}, *c*-C_6H_{10}, and 1,4-*c*-C_6H_8. The measurements were performed using an absolute technique: the discharge flow/laser induced fluorescence.

In parallel with experiments, ab initio calculations (PMP2, HF-DFT, and CASPT2) have been carried out. They give the largest activation energy for reaction 1 (CH_3O + *c*-C_6H_{12} → products 1); in line with experiment; and a good agreement with the experimental results at the CASPT2 level. No clear conclusion can be drawn from ab initio calculations at this stage concerning the absolute rate constants for reaction 2 (CH_3O + *c*-C_6H_{10} → products 2) and reaction 3 (CH_3O + 1,4-*c*-C_6H_8 → products 3) or concerning the dominant pathway for reaction 2. However, the comparison between the results of the calculations presented herein (barrier heights) and those of the experiments endorse increasing reactivity in the series from cyclohexane system to the 1,4-cyclohexadiene system. As for the mechanism, the theoretical study shows that the π electronic system plays an important role in the CH_3O fragment entering pathway.

To sum up, although calculations for reactions 2 and 3 show that the addition channel may play a role in the mechanism, we can favor the abstraction pathway as the main one for the following reasons:

(1) lack of pressure dependence,

(2) clear positive temperature coefficient,

(3) lack of strong trend favoring addition from the theoretical computations.

Obviously, further measurements, for example including the yield of reaction products, should be done to decide which channel is the dominant pathway.

As mentioned in the Introduction another purpose of this work was to provide quantitative data relevant to the barriers for isomerization of large alkoxyl radicals. By analogy with OH abstraction barriers, Atkinson[1] proposed activation energies for isomerizations corresponding to the transfer of an H atom bonded to a primary carbon (35 kJ mol^{-1}), a secondary carbon (28 kJ mol^{-1}), or a tertiary carbon (23 kJ mol^{-1}). The barrier for the H abstraction from a secondary carbon (reaction 1, 24.5 kJ mol^{-1}) obtained in this work supports the qualitative statement of Atkinson. However, more systematic measurements with various bonded H atoms are needed.

Acknowledgment. The I.D.R.I.S. and C.R.I.H.A.N. computing centers are acknowledged for the CPU time facilities. We thank CERLA (Centre d'Etudes et de Recherches Lasers et Applications) for financial support. CERLA is supported by the Ministère chargé de la recherche, Région Nord/Pas-de-Calais and the Fonds Européen de Developpement Economique des Regions (FEDER). The authors appreciate the assistance of Dr. B. Coquart in the revision of the manuscript.

References and Notes

(1) Atkinson, R. *Int. J. Chem. Kinet.* **1997**, *29*, 99.

(2) Fittschen, C.; Delcroix, B.; Gomez, N.; Devolder, P. *J. Chim. Phys.* **1998**, *95*, 2129.

(3) Heicklen, J. *Adv. Photochem.* **1988**, *14*, 177.

(4) Baldwin, A. C.; Barker, J. R.; Golden, D. M.; Hendry, D. G. *J. Phys. Chem.* **1977**, *81*.

(5) Viskolcz, B.; Lendvay, G.; Kortvelyesi, T.; Seres, L. *J. Am. Chem. Soc.* **1996**, *118*, 3006.

(6) Lendvay, G.; Viskolcz, B. *J. Phys. Chem. A* **1998**, *102*, 10777.

(7) Biggs, P.; Canosa-Mas, C. E.; Fracheboud, J. M.; Shallcross, D. E.; Wayne, R. P. *J. Chem. Soc., Faraday Trans.* **1997**, *93*, 2481.

(8) Devolder, P.; Fittschen, C.; Frenzel, C.; Hippler, H.; Poskrebyshev, G.; Striebel, F.; Viskolcz, B. *Phys. Chem. Chem. Phys.* **1999**, *1*, 675.

(9) Caralp, F.; Devolder, P.; Fittschen, C.; Gomez, N.; Hippler, H.; Méreau, R.; Rayez, M.-T.; Striebel, F.; Viskolcz, B. *Phys. Chem. Chem. Phys.* **1999**, *1*, 2935.

(10) Eyring, H. *J. Chem. Phys* **1935**, *3*, 107.

(11) Inoue, G.; Akimoto, H.; Okuda, M. *J. Chem. Phys.* **1980**, *72*, 1769.

(12) Butler, J. E. *Appl. Opt.* **1982**, *21*, 3617.

(13) Mazur, E. *Rev. Sci. Instrum.* **1986**, *57*, 2507.

(14) Durant, L. J. *J. Phys. Chem.* **1991**, *95*, 10701.

(15) Dobe, S.; Berces, T.; Temps, F.; Wagner, H. G.; Ziemer, H. *The 20th Symposium of Combustion*, The Combustion Institute: Pittsburgh, PA, 1994.

(16) Biggs, P.; Canosa-Mas, C. E.; Fracheboud, J. M.; Parr, A. D.; Shallcross, D. E.; Wayne, R. P.; Caralp, F. *J. Chem. Soc., Faraday Trans.* **1993**, *89*, 4163.

(17) Caralp, F.; Rayez, M.-T.; Forst, W.; Gomez, N.; Delcroix, B.; Fittschen, C.; Devolder, P. *J. Chem. Soc., Fraday Trans.* **1998**, *94*, 3321.

(18) Keyser, L. F. *J. Phys. Chem.* **1984**, *88*, 4750.

(19) Gomez, N. *Etudes cinétiques de quelques réactions bimoléculaires de CH_3O et de la décomposition thermique unimoléculaire de C_2H_5O*. Ph.D. Thesis, Université des Sciences et Technologies de Lille, Lille, France, 1999.

(20) Frisch, M. J.; Trucks, G. W.; Schlegel, H. B.; Gill, P. M. W.; Johnson, B. G.; Robb, M. A.; Cheeseman, J. R.; Keith, T.; Petersson, G. A.; Montgomery, J. A.; Raghavachari, K.; Al-Laham, M. A.; Zakrzewski, V. G.; Ortiz, J. V.; Foresman, J. B.; Cioslowski, J.; Stefanov, B. B.; Nanayakkara, A.; Challacombe, M.; Peng, C. Y.; Ayala, P. Y.; Chen, W.; Wong, M. W.; Andres, J. L.; Replogle, E. S.; Gomperts, R.; Martin, R. L.; Fox, D. J.; Binkley, J. S.; Defrees, D. J.; Baker, J.; Stewart, J. P.; Head-Gordon, M.; Gonzalez, C.; Pople, J. A. *Gaussian 94*, revision D.4; Gaussian, Inc.: Pittsburgh, PA, 1995.

(21) Lee, C.; Yang, W.; Parr, R. *Phys. Rev. B* **1988**, *37*, 785.

(22) Miehlich, B.; Savin, A.; Stoll, H.; Preuss, H. *Chem. Phys. Lett.* **1989**, *157*, 200.

(23) Becke, A. *J. Chem. Phys.* **1993**, *98*, 5648.

(24) Woon, D.; Dunning, T. H. *J. Chem. Phys.* **1993**, *98*, 1358.

(25) Kendall, R.; Dunning, T. H.; Harrison, R. *J. Chem. Phys.* **1992**, *96*, 6796.

(26) Dunning, T. H. *J. Chem. Phys.* **1989**, *90*, 1007.

(27) Schaftenaar, G.; Noordik, J. *J. Comput.-Aided Mol. Design* **2000**, *14*, 123.

(28) *Molcas*, version 4; Andersson, K.; Blomberg, M. R. A.; Fulscher, M.; Karlstrom, G.; Lindh, R.; Malmqvist, P. A.; Neogrady, P.; Olsen, J.; Roos, B.; Sadlej, A.; Schutz, M.; Seijo, L.; Serrano-Andres, L.; Siegbahn, P. E. M.; Widmark, P. O.; University of Lund, Sweden, 1997.

(29) Hehre, W. J.; Radom, L.; Schleyer, P. v. R.; Pople, J. A. *Ab Initio Molecular Orbital Theory;* John Wiley & Sons: New York, 1986.
(30) Roos, B. O.; Andersson, K.; Fulscher, M. P.; Malmqvist, P.-A.; Serrano-Andres, L.; Pierloot, K.; Merchan, M. *Advances in Chemical Physics*; John Wiley & Sons: New York, 1996; Vol. XCIII.
(31) Andersson, K. In *Encyclopedia of Computational Chemistry*; Wiley: New York, 1998; p 460.
(32) Andersson, K.; Malmqvist, P.-A.; Roos, B.; Sadlej, A. J.; Wolinski, K. *J. Phys. Chem.* **1990**, *94*, 5483.
(33) Andersson, K.; Malmqvist, P. A.; Roos, B. *J. Chem. Phys.* **1992**, *96*, 1218.
(34) Postat, B.; Henon, E.; Auge, F.; Bohr, F. *KISTHEP*; Université de Reims, 1997.
(35) Chuang, Y.-Y.; Corchado, J.; Fast, P.; Villa, J.; Coitino, E. L.; Hu, W.-P.; Liu, Y.-P.; Lynch, G. C.; Nguyen, K. A.; Jackels, C. F.; Gu, M. Z.; Rossi, I.; Clayton, S.; Melissas, V. S.; Steckler, R.; Garrett, B. C.; Isaacson, A. D.; Truhlar, D. G. *POLYRATE*, version 8.0; University of Minnesota, Minneapolis, 1998.
(36) Wigner, E. *Z. Phys. Chem. B* **1932**, *19*, 203.
(37) Isaacson, A. D.; Garrett, B. C. In *The Theory of Chemical Reaction Dynamics*; Baer, M., Ed.; CRC Press: Boca Raton, FL, 1985; Vol. 4.
(38) Truhlar, D. G.; Kuppermann, A. *J. Chem. Phys.* **1970**, *52*, 3842.
(39) Truhlar, D. G.; Kuppermann, A. *J. Am. Chem. Soc.* **1971**, *93*, 1840.
(40) Garrett, B. C.; Truhlar, D. G.; Grev, R. S.; Magnuson, A. W. *J. Phys. Chem.* **1980**, *84*, 1730.
(41) Atkinson, R. *J. Chem. Phys. Ref. Data* **1997**, *26*, 215.
(42) Ohta, N. *Int. J. Chem. Kinet.* **1984**, *16*, 1495.
(43) Henon, E.; Bohr, F. *Chem. Phys. Lett.* In press.
(44) Bohr, F.; Brion, J.; Delcroix, B.; Devolder, P.; Fittschen, C.; Gomez, N.; Henon, E. *EUROTRAC*, Symposium 98; Witpress: Southampton, U.K., 1999.